DOI: 10.1002/ejic.201000206

Diastereoselective Assembly of Helicates Incorporating a Hexadentate Chiral Scaffold

Edwin C. Constable,*[a] Guoqi Zhang,[a] Catherine E. Housecroft,*[a] Markus Neuburger,[a] and Jennifer A. Zampese[a]

Keywords: Helical structures / Stereochemistry / Chirality / N ligands / Copper / Iron / Zinc

The condensation of enantiopure (1*R*,2*R*)-(–)-1,2-diaminocyclohexane with two equivalents of 2,2′-bipyridine-6-carbaldehyde followed by reduction with $NaBH_4$ allows the facile synthesis of the enantiopure hexadentate ligand (*R*,*R*)-**3**. Each tridentate metal-binding domain in (*R*,*R*)-**3** exhibits a degree of flexibility arising from inversion at the amine nitrogen centre and rotation about N–C and C–C single bonds. This leads to the formation of either *M*-$[M\{(R,R)\text{-}\mathbf{3}\}]^{2+}$ or *P*-$[M\{(R,R)\text{-}\mathbf{3}\}]^{2+}$. The solid-state structures of the copper(II), iron(II) and zinc(II) complexes of (*R*,*R*)-**3** all show a preference for *M*-$[M\{(R,R)\text{-}\mathbf{3}\}]^{2+}$. In solution, $[Fe\{(R,R)\text{-}\mathbf{3}\}]^{2+}$ exists predominantly as one diastereoisomer (assumed to be the *M*-form). The preference for the *M*- over *P*-form is rationalized in terms of a favourable *anti* configuration of the NH and cyclohexane-1,2-diyl CH hydrogen atoms in the *M*-form, and an unfavourable *syn*-configuration in the *P*-form. When (*R*,*R*)-**4**, the Schiff base analogue of (*R*,*R*)-**3**, combines with zinc(II) or silver(I), [2+2] double helicates with *M*-chirality assemble in the solid state. With (*S*,*S*)-**4**, iron(II) also assembles into a dinuclear, double helicate with *M*-handedness. Complete stereoselectivity is observed in solution with NMR spectroscopic data indicating the presence of one diastereoisomer. The preference for a dinuclear over mononuclear helicate can be traced to a decrease in ligand flexibility on going from **3** (saturated backbone) to **4** (unsaturated imine backbone).

Introduction

The study of main group (dominantly C, N, P or S) stereogenic centres is a well-established, classical discipline.[1] Less commonly studied are compounds in which the chirality is associated with a metal centre.[2] Although an octahedral $[MABCDEF]^{n+}$ compound is expected to be chiral,[3] few examples of such stereochemically complex species have been prepared.[4–6] The most common examples of chiral octahedral complexes are those of the type $[ML_3]^{n+}$ and *cis*-$[ML_2X_2]^{n+}$ with chelating bidentate ligands L.[7,8] By using enantiopure chiral ligands, it is possible to obtain complexes with stereogenic metal centres in high diastereomeric excess.[8–10] Among the multitopic ligands used to direct the configuration of stereogenic metal centres in complexes,[11] oligopyridine and 1,10-phenanthroline metal-binding domains are common choices and a range of chiral derivatives has been reported.[12–15] The family of chiragens derived from naturally occurring terpenes and designed by von Zelewsky[16,17] has been widely investigated. These and other oligopyridine-based chiral ligands reported to date usually possess a chiral auxillary fused to one pyridine ring, and achiral spacers linking the chiral metal-binding domains. However, a disadvantage of these ligands is that their syntheses are non-trivial.

In principle, enantioselectivity for an octahedral metal complex can also be attained by using a chiral, hexadentate ligand which binds to the metal through all six donor atoms. Previous studies in this area have involved the use of a chiral scaffold to which metal-binding domains are attached, specifically three bidentate domains on a C_3-scaffold,[18–20] or two tridentate units on a C_2-scaffold.[21–23] Atropisomeric scaffolds, most commonly those based on a biaryl core, are ubiquitous in the design of ligands for asymmetric catalysis[24–26] and the application in coordination and metallosupramolecular chemistries of chiral ligands built upon 1,1′-binaphthyl-2,2′-diol and 2,2′-diamino-1,1′-binaphthyl scaffolds has been reviewed.[27] The combination of a 1,1′-binaphthalene core with pendant oligopyridine or related metal-binding domains is less well explored.[21–23,28–34] Over ten years ago, Hannon noted that the high-yield synthesis of imines from reactions of aldehydes with amines gives a convenient route to imine-based ligands for supramolecular assemblies.[35] This methodology has been employed for the formation of chiral **1**[32,33] and **2**[34] (Scheme 1), and we have recently described[34] the ability of enantiomerically pure (*R*)-**2** and (*S*)-**2** to bind iron(II) with complete control of the stereochemistry at the stereogenic metal centre.

[a] Department of Chemistry, University of Basel, Spitalstrasse 51, 4056 Basel, Switzerland
Fax: +41-61-267-1008
E-mail: Catherine.Housecroft@unibas.ch
edwin.constable@unibas.ch

Supporting information for this article is available on the WWW under http://dx.doi.org/10.1002/ejic.201000206.

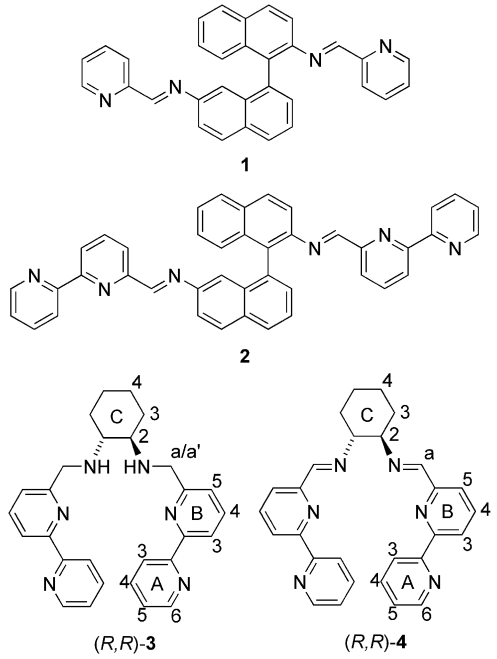

Scheme 1. Ligand structures and atom numbering for NMR spectroscopic assignments in ligands **3** and **4**.

Amine–aldehyde condensation is routinely applied to the facile synthesis of chiral Schiff base ligands, and it is well documented in the catalytic literature.[36] We have recently reported their use in the development of highly enantioselective catalysts for the asymmetric Henry reaction.[37–39] Most commonly, such ligands feature an *O*,*N*,*N*′,*O*′-donor set. The introduction of a chiral auxillary into a salen-type backbone has been shown to direct the assembly of a supramolecular helix around a lanthanoid centre.[40]

We now report the synthesis and characterization of the enantiomerically pure hexadentate ligand (*R*,*R*)-**3** and illustrate its use to provide stereochemical control at octahedral metal centres in mononuclear helicates. We also describe how moving from the saturated backbone of (*R*,*R*)-**3** to the imine-containing (*R*,*R*)-**4** and (*S*,*S*)-**4** switches the stereochemical control from a single to double helical assembly.

Results and Discussion

Reduced Schiff Base Ligand (*R*,*R*)-3

The condensation of two equivalents of 2,2′-bipyridine-6-carbaldehyde with (1*R*,2*R*)-(–)-1,2-diaminocyclohexane yielded the Schiff base ligand (*R*,*R*)-**4** (Scheme 2). However, on standing in air at room temperature the white solid turned to a yellow oil within two days and could not be fully characterized. When the Schiff base was reduced in situ using $NaBH_4$, (*R*,*R*)-**3** (Scheme 1) was isolated in 64% yield as an oil ($[\alpha]_D^{20}$ = –77.8). The ESI mass spectrum of (*R*,*R*)-**3** exhibited a base peak at *m*/*z* 473.3 corresponding to the ion $[M + Na]^+$ and a lower intensity peak at *m*/*z* 451.5 assigned to $[M + H]^+$. The ^1H and ^{13}C NMR spectra of the product were in accord with the structure shown in Scheme 1; Figure S1 depicts the ^1H NMR spectrum. The diastereotopic CH_2 group (H^a and $H^{a'}$) gives rise to doublets at δ 3.96 and 4.16 ppm (J = 14.4 Hz). The bpy proton signals were assigned from the COSY and NOESY spectra, the signals for H^{B3} and H^{B5} being distinguished by the appearance of NOESY cross peaks between H^{B3} and H^{A3}, and between H^{B5} and H^a/$H^{a'}$. ^1H and ^{13}C NMR spectroscopic signals for the cyclohexane-1,2-diyl ring protons were assigned using COSY, NOESY, HMQC and HMBC techniques. In the ^{13}C NMR spectrum, the signal for C^{B6} at δ 158.8 ppm was poorly resolved, but HMBC cross peaks to protons H^{B4} and H^a/$H^{a'}$ permitted an unambiguous assignment.

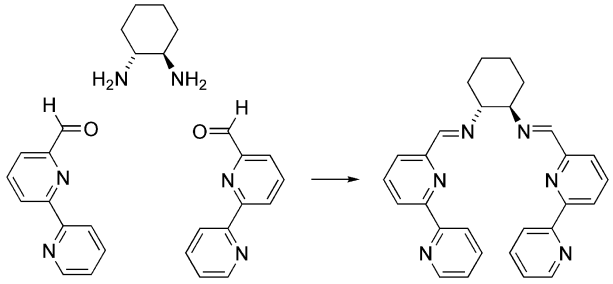

Scheme 2. Formation of the Schiff base (*R*,*R*)-**4**.

Synthesis and Characterization of Copper(II), Iron(II) and Zinc(II) Complexes of (*R*,*R*)-3

Treatment of (*R*,*R*)-**3** with $Zn(OAc)_2{\cdot}1.5H_2O$ or $Cu(OAc)_2$ followed by anion exchange resulted in the formation of $[Zn\{(R,R)\text{-}\mathbf{3}\}][PF_6]_2$, $[Cu\{(R,R)\text{-}\mathbf{3}\}][PF_6]_2$, while $[Fe\{(R,R)\text{-}\mathbf{3}\}][BF_4]_2$ was prepared by the reaction between $[Fe(OH_2)_6][BF_4]_2$ and (*R*,*R*)-**3**. All complexes were formed in good or excellent yield. The base peak in the ESI mass spectrum of $[Zn\{(R,R)\text{-}\mathbf{3}\}][PF_6]_2$ was assigned to $[M - PF_6]^+$ (*m*/*z* = 659.6), and loss of a second anion was also observed (*m*/*z* = 257.4 assigned to $[M - 2PF_6]^{2+}$). Similar behaviour was observed in the ESI mass spectra of $[Cu\{(R,R)\text{-}\mathbf{3}\}][PF_6]_2$ and $[Fe\{(R,R)\text{-}\mathbf{3}\}][BF_4]_2$. The CD spectra of CH_2Cl_2 solutions of $[Zn\{(R,R)\text{-}\mathbf{3}\}][PF_6]_2$, $[Cu\{(R,R)\text{-}\mathbf{3}\}][PF_6]_2$ and $[Fe\{(R,R)\text{-}\mathbf{3}\}][BF_4]_2$ are compared with that of the free ligand (*R*,*R*)-**3** in Figure S2.

X-ray quality colourless needles of $[Zn\{(R,R)\text{-}\mathbf{3}\}][PF_6]_2$, blue-green prisms of $[Cu\{(R,R)\text{-}\mathbf{3}\}][PF_6]_2$, and black blocks of $[Fe\{(R,R)\text{-}\mathbf{3}\}][BF_4]_2$ were grown by slow diffusion of Et_2O into a MeCN solution of each complex over a period of 2 weeks. Each compound crystallizes in the orthorhombic, chiral $P2_12_12_1$ space group, and Figure 1, Figure 2, and Figure 3 illustrate that each cation exhibits *M*-stereochemistry at the metal centre. The two hexafluoridophosphate salts are isostructural. Since the bpy units are essentially planar, and the C and N atoms of the attached CH_2NH units lie within 0.35 Å of the least-squares plane through each tridentate domain, the pitch of the helix defined by the coordinated ligand can be assessed from the angles N2–N3–N4 and N3–N4–N5. For $[Cu\{(R,R)\text{-}\mathbf{3}\}]^{2+}$ and $[Zn\{(R,R)\text{-}\mathbf{3}\}]^{2+}$, these angles lie in the range 74.6–81.1°,

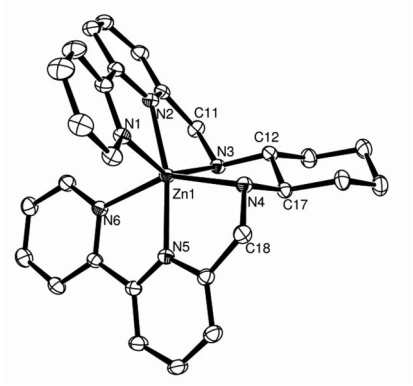

Figure 1. Structure of the *M*-[Zn{(*R*,*R*)-**3**}]$^{2+}$ cation in *M*-[Zn{(*R*,*R*)-**2**}][PF_6]$_2$ with ellipsoids plotted at the 50% probability level. Selected bond lengths and angles: Zn1–N1 2.2202(8), Zn1–N2 2.0812(7), Zn1–N3 2.2002(8), Zn1–N4 2.1662(7), Zn1– N5 2.0750(8), Zn1–N6 2.2503(8), N3–C11 1.471(1), N4–C18 1.474(1) Å; N1–Zn1–N2 75.15(3), N2–Zn1–N3 76.80(3), N3–Zn1–N4 81.58(3), N4–Zn1–N5 78.30(3), N5–Zn1–N6 74.69(3)°.

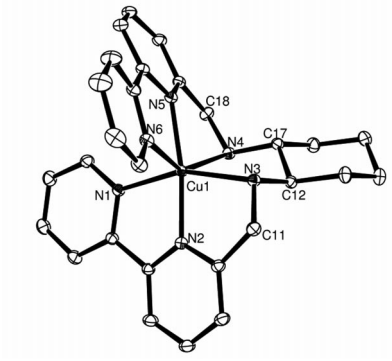

Figure 2. Structure of the *M*-[Cu{(*R*,*R*)-**3**}]$^{2+}$ cation in *M*-[Cu{(*R*,*R*)-**2**}][PF_6]$_2$ with ellipsoids plotted at the 40% probability level. Selected bond parameters: Cu1–N1 2.092(1), Cu1–N2 1.9442(9), Cu1–N3 2.1164(9), Cu1–N4 2.2940(9), Cu1–N5 2.0378(9), Cu1–N6 2.3454(9), N4–C18 1.459(1), N3–C11 1.482(1) Å; N1–Cu1–N2 79.29(3), N2–Cu1–N3 80.32(4), N3–Cu1–N4 79.95(3), N4–Cu1–N5 76.23(3), N5–Cu1–N6 74.87(3)°.

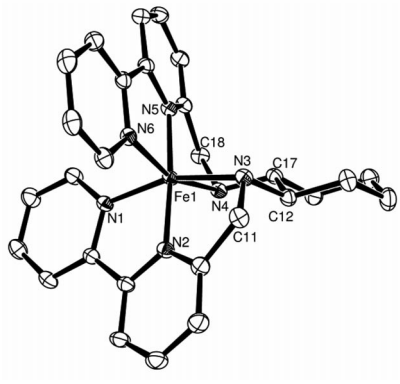

Figure 3. Structure of the *M*-[Fe{(*R*,*R*)-**3**}]$^{2+}$ cation in *M*-[Fe{(*R*,*R*)-**3**}][BF_4]$_2$; ellipsoids are plotted at the 40% probability level. Selected bond lengths and angles: Fe1–N1 1.976(1), Fe1–N2 1.890(1), Fe1–N3 2.043(1), Fe1–N4 2.043(1), Fe1–N5 1.889(1), Fe1–N6 1.964(1), N3–C11 1.490(2), N4–C18 1.484(2) Å; N1–Fe1–N2 81.11(6), N2–Fe1–N3 80.60(6), N3–Fe1–N4 84.23(5), N4–Fe1–N5 80.10(6), N5–Fe1–N6 80.99(6)°.

while for [Fe{(*R*,*R*)-**3**}]$^{2+}$, they are 70.9 and 71.5°. The difference is consistent with the shorter Fe–N bond lengths [1.889(1)–2.043(1) Å] compared to the Cu–N and Zn–N distances [1.9442(9)–2.3454(9) Å], but may also be a consequence of differences in packing on going from the [PF_6]$^-$ to [BF_4]$^-$ counterion. In all three structures, the solid state packing is dominated by N–H···F and C–H···F interactions.

Control of Stereochemistry in Metal Complexes of (*R*,*R*)-3

The solid-state structural data presented above provide evidence for a stereochemical preference for the *M*-[M{(*R*,*R*)-**3**}]$^{2+}$ cation for M = Fe, Cu and Zn. We were, therefore, interested in seeing whether this stereochemical discrimination also existed in solution. Solution ^{1}H and ^{13}C NMR spectra were recorded for the diamagnetic zinc(II) and iron(II) complexes. Metal binding by ligand (*R*,*R*)-**3** is accompanied by the expected shift of the signal for bpy proton H^{A6} to lower frequency: δ 8.60 to 7.72 ppm and δ 8.60 to 6.82 ppm for the zinc(II) and iron(II) complexes, respectively (for the ligand in $CDCl_3$, see Figure S1, and complexes in CD_3CN). In the free ligand, the signal for the NH proton is very broad, and no coupling is observed between the NH and adjacent CH_2 group or the adjacent cyclohexane-1,2-diyl CH proton. In contrast, the ^{1}H NMR spectrum for [Fe{(*R*,*R*)-**3**}][BF_4]$_2$ exhibits a fairly sharp NH signal, and for [Zn{(*R*,*R*)-**3**}][PF_6]$_2$, this resonance appears as a fairly well-resolved doublet of doublets (J = 10.5 Hz to cyclohexane-1,2-diyl proton H^{C2} and J = 5.9 Hz to methylene H^a). The signals for the diastereotopic protons H^a and $H^{a'}$ appear as a doublet of doublets and as a doublet, respectively, in both complexes. The COSY spectrum confirmed coupling between one $H^{a/a'}$ and NH. The ^{1}H and ^{13}C NMR spectra of [Zn{(*R*,*R*)-**3**}][PF_6]$_2$ and [Fe{(*R*,*R*)-**3**}][BF_4]$_2$ were fully assigned by two-dimensional methods.

Despite sequential recrystallizations of [Fe{(*R*,*R*)-**3**}][BF_4]$_2$, the ^{1}H NMR spectrum showed a subspectrum with the same spectroscopic signature as that of [Fe{(*R*,*R*)-**3**}]$^{2+}$. The COSY spectrum confirmed the same relationship between peaks in the subspectrum as in the dominant component. After one recrystallization, the ratio of integrals of pairs of corresponding peaks was 4:1 (Figure 4) and this ratio was reproduced in two separate syntheses of the

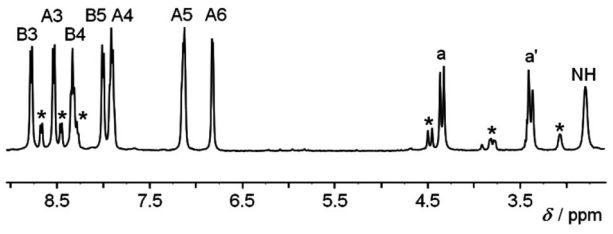

Figure 4. 400 MHz ^{1}H NMR spectrum of CD_3CN solution (room temperature) of [Fe{(*R*,*R*)-**3**}][BF_4]$_2$ after one crystallization. The signals marked by * are assigned to a second diastereoisomer.

iron(II) complex. After a second recrystallization, the ratio changed to approximately 6:1, and after a third recrystallization was about 12:1. The ^{1}H NMR spectrum of [Zn{(*R*,*R*)-**3**}][PF_6]$_2$ showed only minor traces (< 4%) of a second component, even before recrystallization, consistent with better stereochemical selectivity in the case of zinc(II) compared to iron(II), or higher lability in the case of iron(II).

The description and origin of the chirality in the metal complexes of ligand **3** are of interest. The free ligand possesses two stereogenic centres (assuming rapid inversion at the amine nitrogen atom) giving rise to the three diastereoisomers (*R*,*R*), (*S*,*S*) and (*R*,*S*). In this work we have used the enantiomerically pure (*R*,*R*)-diastereoisomer. Each [M(**3**)]$^{2+}$ metal complex could be described in terms of three, four or five stereogenic centres, relating to (i) the two carbon stereogenic centres in the ligand [fixed as (*R*,*R*) in this case], (ii) the configuration at the coordinated amine nitrogens which, when bound to the metal centre, can no longer freely invert, and (iii) the helicity at the metal with conventional *P*/*M* notation. Occam's razor[41] indicates that the preferred description is in terms of three stereogenic centres and we adopt the description *P*-(*R*,*R*) and *M*-(*R*,*R*) for the diastereoisomeric complexes. The helicity at the metal centre defines the stereochemistry at the two amine nitrogens which must adopt either an (*R*,*R*) or (*S*,*S*) configuration (Scheme 3); the (*R*,*S*) configuration is precluded on steric grounds. Thus, although we use three stereogenic centre descriptors, it is more convenient to discuss the stability of the diastereoisomers in terms of the configuration at the nitrogen atoms (vide infra). In the structurally characterized *M*-[M{(*R*,*R*)-**3**}]$^{2+}$ diastereoisomers, each amine nitrogen atom exhibits an (*S*)-configuration, and the NH and H^{C2} (Scheme 1) hydrogen atoms are in an *anti*-configuration. The change in configuration at the metal centre on going to *P*-[M{(*R*,*R*)-**3**}]$^{2+}$ necessarily requires that each amine nitrogen atom has to be in an (*R*)-configuration and the NH and H^{C2} hydrogen atoms are then forced into an unfavourable *syn*-configuration. The energy minimized[42] structures of *M*-[M{(*R*,*R*)-**3**}]$^{2+}$ and *P*-[M{(*R*,*R*)-**3**}]$^{2+}$ (in which all M–N bond lengths are 2.0 ± 0.1 Å) allow a comparison of close H···H contacts, and in Table 1, these are compared with the observed contacts in *M*-[Fe{(*R*,*R*)-**3**}][BF_4]$_2$. In fact, the calculated energies of the two minimized structures are very similar, with the *M*,*R*,*R*-diastereoisomer being only marginally preferred over the *P*,*R*,*R*-diastereoisomer.

We rationalize the solution NMR spectroscopic data by the presence of one dominant diastereoisomer, assumed to be *M*-[Fe{(*R*,*R*)-**3**}][BF_4]$_2$, and smaller amounts of *P*-[Fe{(*R*,*R*)-**3**}][BF_4]$_2$. The stereochemical control in the case of the zinc(II) centre appears to be greater than that in the iron(II) complex. The increased helical pitch (see structural description) for the former would necessarily impose closer unfavourable H···H contacts. No cross peaks between the peaks assigned to the two diastereoisomers were observed in the EXSY spectrum, indicating that the interconversion is slow on the NMR timescale.

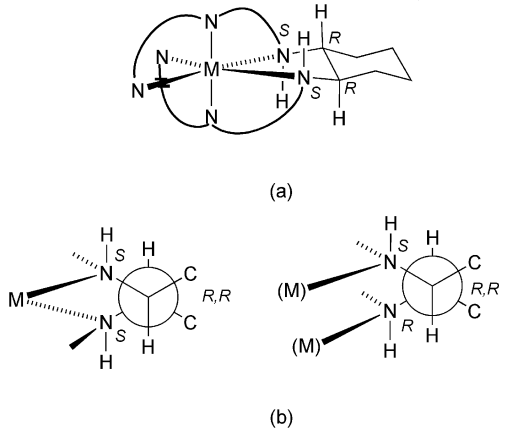

Scheme 3. (a) Diagram of one of the diastereoisomers showing the various steregenic centres. In the diagram shown, the metal has *M*-chirality. (b) Representations of the stereochemistry at nitrogen in a Newman projection along the C–C bond of the cyclohexane showing that the *meso* (*R*,*S*) configuration cannot chelate to the metal.

Table 1. Short H···H contacts in modelled *M*-[M{(*R*,*R*)-**3**}]$^{2+}$ and *P*-[M{(*R*,*R*)-**3**}]$^{2+}$ and in the crystallographically determined structure of *M*-[Fe{(*R*,*R*)-**3**}][BF_4]$_2$. For consistency, the H atom numbering scheme is that shown in Scheme 1.

Contacts	*M*-[M{(*R*,*R*)-**3**}]$^{2+}$ modelled /Å	*P*-[M{(*R*,*R*)-**3**}]$^{2+}$ modelled /Å	*M*-[Fe{(*R*,*R*)-**3**}][BF_4]$_2$ /Å
H^{C3}···H^a	2.4	2.5	2.2
H^{C2}···H^a	2.4		2.5
$H^{C3'}$···H^{NH}	2.3		2.5
H^{C2}···H^{NH} (*syn*)		2.2	
$H^{C3'}$···H^a		2.1	

Figure 5 depicts the electronic absorption spectra of MeCN solutions of the complexes. The high energy bands common to all three complexes are assigned to ligand-based π*←π transitions. In addition, [Fe{(*R*,*R*)-**3**}]$^{2+}$ exhibits a lower energy absorption at 373 nm and an MLCT band at 578 nm.

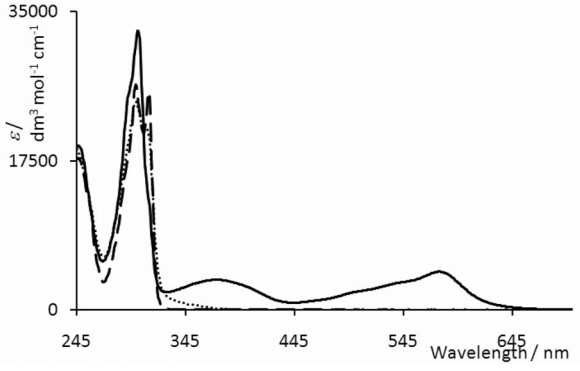

Figure 5. Electronic absorption spectra of MeCN solutions (5.0×10^{-5} mol dm^{-3}) of [Fe{(*R*,*R*)-**3**}][BF_4]$_2$ (—), [Cu{(*R*,*R*)-**3**}][PF_6]$_2$ (····) and [Zn{(*R*,*R*)-**3**}][PF_6]$_2$ (- - -).

One-Pot Syntheses of Double Helical Metal Complexes of (*R*,*R*)-4 and (*S*,*S*)-4

We have previously reported how Schiff base ligands (*S*)-**2** and (*R*)-**2** which contain a 1,1′-binaphthyl scaffold direct the spatial properties of the two bpy-containing arms of the ligands, completely defining the stereochemistry of the iron(II) complexes *M*-[Fe{(*S*)-**2**}]$^{2+}$ and *P*-[Fe{(*R*)-**2**}]$^{2+}$.[34] On the other hand, (*R*,*R*)-**3**, containing a cyclohexane-1,2-diyl backbone, is saturated and each tridentate metal-binding domain has a degree of flexibility arising from inversion at the amine nitrogen centre and rotation about the single bonds in the saturated spacers. This allows the formation of either *M*-[M{(*R*,*R*)-**3**}]$^{2+}$ or *P*-[M{(*R*,*R*)-**3**}]$^{2+}$, with complete stereochemical control being observed in the structural determination, but with discrimination being metal-dependent in solution. We were intrigued to know how the stereochemical control would be affected by limiting the flexibility of the ligand. This prompted an investigation of the coordination behaviour of Schiff base ligand **4** by applying a one-pot approach using the metal ion to template the formation of diimine **4**. This strategy has been successfully employed in the reactions of (*R*)- or (*S*)-2,2′-diamino-1,1′-binaphthyl with pyridine-2-carbaldehyde in the presence of Ag^I or Cu^I ions to produce enantiopure dinuclear double helicates.[32] The related Schiff base ligand prepared from (1*R*,2*R*)-(–)- or (1*S*,2*S*)-(+)-1,2-diaminocyclohexane and quinoline-2-carbaldehyde is similarly preorganized for the assembly of [2+2] double helicates, although in this case, the free ligand was prepared prior to its reaction with copper(I) ions.[43] Both these studies[32,43] utilize diimine ligands containing two bidentate metal-binding domains and evidence stereochemical control at four-coordinate metal centres. In contrast, a wider range of metal ions can be targeted using hexadentate Schiff base ligand **4**.

The reactions of (1*R*,2*R*)-(–)- or (1*S*,2*S*)-(+)-1,2-diaminocyclohexane with two equivalents of 2,2′-bipyridine-6-carbaldehyde in the presence of one equivalent of $FeCl_2{\cdot}4H_2O$ resulted, after anion exchange, in the formation of purple solids, elemental analytical data for which confirmed 1:1 metal/ligand **4** ratios. The base peak in the electrospray mass spectrum of a methanol solution of each complex appeared at *m*/*z* 521.2 and corresponded to [Fe(**4**) + F]$^+$. The highest mass peak envelope at *m*/*z* 647.1 exhibited an isotope pattern and peak separation consistent with [Fe_2(**4**)$_2$(PF_6)$_2$]$^{2+}$. Dominant peaks at *m*/*z* 469.3 and 501.2 were assigned to [Na(**4**)]$^+$ and [Na(**4**) + MeOH]$^+$. The positive-mode FAB mass spectrum exhibited peaks at *m*/*z* 1439.3, 1293.8 and 1149.9 which were consistent with the ions [Fe_2(**4**)$_2$(PF_6)$_3$]$^+$, [Fe_2(**4**)$_2$(PF_6)$_2$]$^+$ and [Fe_2(**4**)$_2$(PF_6)]$^+$. Single, X-ray quality crystals of the complex containing (*S*,*S*)-**4** were grown by diffusion of Et_2O over a period of one day into an acetone/acetonitrile solution of the compound. The complex crystallizes in the chiral space group $P2_12_12$. The structure determination confirmed the formation of the [2+2] double helical cation shown in Figure 6, with each of the two tridentate donor sets of (*S*,*S*)-**4** directed to a different iron(II) ion. The preference for this assembly over the [1+1] motif shown in Figure 3 for *M*-[Fe{(*R*,*R*)-**3**}]$^{2+}$ is consistent with the decrease in ligand flexibility on going from **3** to **4**. The double helicate in Figure 6 exhibits *M*-handedness (Scheme 4), and the pitch of the helix is such that the Fe···Fe separation is 5.2898(12) Å. The Fe–N bond lengths in the *M*-[Fe_2{(*S*,*S*)-**4**}$_2$]$^{4+}$ cation lie within a similar range to those in *M*-[Fe{(*R*,*R*)-**3**}]$^{2+}$. Each cyclohexanedyl unit nessles within a V-shaped cavity between two bpy domains and this structural feature is pertinent to the NMR spectroscopic discussion below. There is no π-stacking between bpy units within a cation, although the imino N=CH units lie over one another at a distance of ≈ 3.4 Å. The overall packing is dominated by C–H···F, C–H···N, and C–H···O interactions, and there is no intercation π-stacking.

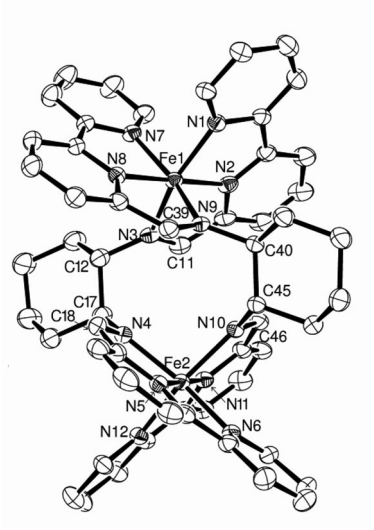

Figure 6. Structure of the *M*-[Fe_2{(*S*,*S*)-**4**}$_2$]$^{4+}$ cation in 4[Fe_2{(*S*,*S*)-**4**}$_2$][PF_6]$_4{\cdot}4Et_2O{\cdot}6Me_2CO{\cdot}7MeCN{\cdot}4H_2O$ (ellipsoids plotted at 40% probability level); H atoms omitted. Bond parameters in the coordination spheres: Fe1–N2 1.869(2), Fe1–N8 1.880(2), Fe1–N9 1.975(2), Fe1–N1 1.976(2), Fe1–N7 1.977(2), Fe1–N3 1.979(2), Fe2–N11 1.873(2), Fe2–N5 1.882(2), Fe2–N4 1.973(2), Fe2–N6 1.974(2), Fe2–N10 1.978(2), Fe2–N12 1.985(2) Å; N2–Fe1–N1 80.39(10), N2–Fe1–N3 81.07(10), N8–Fe1–N7 80.51(10), N8–Fe1–N9 80.75(9), N5–Fe2–N4 81.04(10), N5–Fe2–N6 80.32(10), N11–Fe2–N10 80.91(10), N11–Fe2–N12 80.31(10)°.

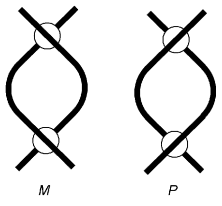

Scheme 4. Schematic representations of *M*- and *P*-double helicates.

The solution electronic absorption spectrum of *M*-[Fe_2{(*S*,*S*)-**4**}$_2$][PF_6]$_4$ (Figure 7) exhibits two MLCT bands at 484 and 604 nm, with a shoulder at 710 nm. There is also a series of intense, high energy absorptions arising from ligand-based π*←π transitions. The fact that the ESI mass spectra of methanol solutions of the iron(II) complexes of

(*S*,*S*)-**4** and (*R*,*R*)-**4** exhibit an $[Fe_2(\mathbf{4})_2(PF_6)_2]^{2+}$ ion as the highest mass peak envelope suggests that the double helical structure is retained in solution. Figure 8 shows the CD spectra of MeCN solutions of $[Fe_2\{(S,S)\text{-}\mathbf{4}\}_2][PF_6]_4$ and $[Fe_2\{(R,R)\text{-}\mathbf{4}\}_2][PF_6]_4$. The data are consistent with either the presence of enantiomerically pure *P*- and *M*-helicates in solution.

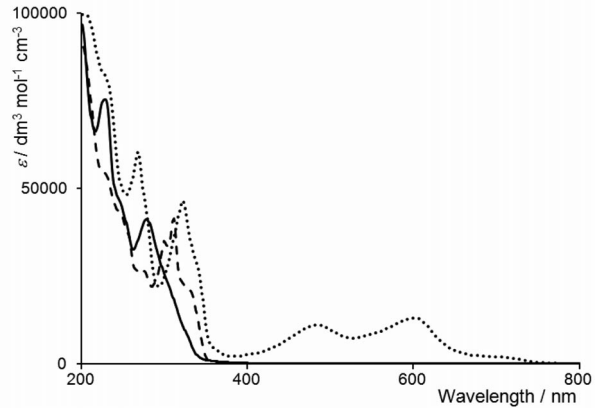

Figure 7. UV/Vis spectra of acetonitrile solutions of $[Fe_2\{(S,S)\text{-}\mathbf{4}\}_2][PF_6]_4$ (····), $[Ag_2\{(R,R)\text{-}\mathbf{4}\}_2][BF_4]_2$ (—), and $[Zn_2\{(R,R)\text{-}\mathbf{4}\}_2][PF_6]_4$ (- - -).

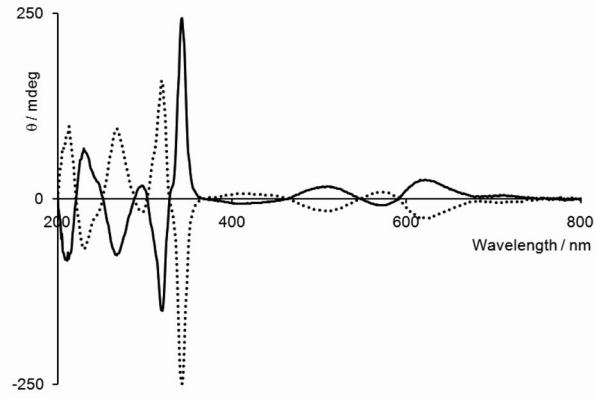

Figure 8. The CD spectra of MeCN solutions (2.5×10^{-5} mol dm^{-3}) of *P*-$[Fe_2\{(R,R)\text{-}\mathbf{4}\}_2][PF_6]_4$ (—) and *M*-$[Fe_2\{(S,S)\text{-}\mathbf{4}\}_2][PF_6]_4$ (····).

The CD_3CN solution ^1H NMR spectra of $[Fe_2\{(S,S)\text{-}\mathbf{4}\}_2][PF_6]_4$ and $[Fe_2\{(R,R)\text{-}\mathbf{4}\}_2][PF_6]_4$ are identical and reveal one ligand environment. Signals in the ^1H and ^{13}C NMR spectra of $[Fe_2\{(S,S)\text{-}\mathbf{4}\}_2][PF_6]_4$ were assigned using COSY, NOESY, HMQC and HMBC methods, and part of the ^1H NMR spectrum is shown in Figure 9. The octahedral coordination environment around the iron(II) centre places proton H^{A6} over the π-cloud of ring B of an adjacent bpy ligand (Figure 9), resulting in a low frequency chemical shift of δ 6.69 ppm. However, in terms of the solution structure, the most diagnostic feature of the ^1H NMR spectrum is the appearance of one of the cyclohexanedyl proton signals at δ = –0.49 ppm. This signal was assigned by 2D-techniques to proton $H^{C3'}$, and its shielding is consistent with the retention of the double helicate in solution with $H^{C3'}$ facing the π-ring current of bpy ring A (Figure 9). The ^1H NMR spectra of $[Fe_2\{(S,S)\text{-}\mathbf{4}\}_2][PF_6]_4$ and $[Fe_2\{(R,R)\text{-}\mathbf{4}\}_2][PF_6]_4$ are consistent with the double helical structures of *M*-$[Fe_2\{(S,S)\text{-}\mathbf{4}\}_2]^{4+}$ and *P*-$[Fe_2\{(R,R)\text{-}\mathbf{4}\}_2]^{4+}$ being preserved in solution, and with the presence of only one diastereoisomer in each case. Note that in the solid state, the lack of crystallographically imposed symmetry means that the members of each set of four protons (e.g. the four H^{A6} protons) are non-equivalent, but the differences are very small.

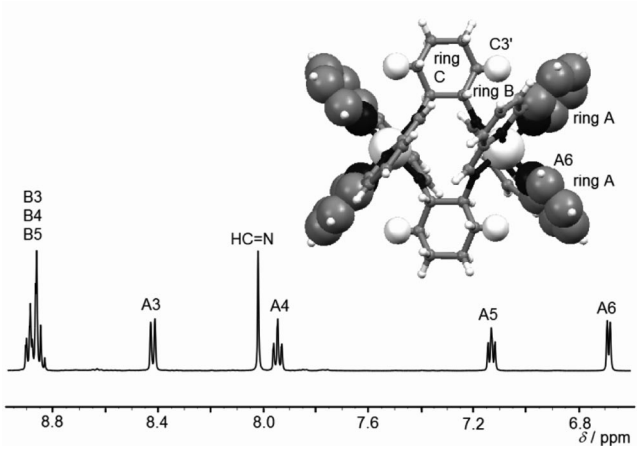

Figure 9. Part of the 500 MHz ^1H NMR spectrum of a CD_3CN solution of $[Fe_2\{(S,S)\text{-}\mathbf{4}\}_2][PF_6]_4$ at room temperature. In the double helical structure of *M*-$[Fe_2\{(S,S)\text{-}\mathbf{4}\}_2]^{4+}$ (drawn using X-ray crystallographic data), each cyclohexanedyl proton $H^{C3'}$ points into the π-cloud of a bpy ring A, and bpy proton H^{A6} faces the π-cloud of a bpy ring B.

The coordination of ligands (*S*,*S*)-**4** and (*R*,*R*)-**4** with iron(II) exemplifies the ability of the ligands to complement the requirements of an octahedral metal ion. We next looked at how ligand (*R*,*R*)-**4** would bind zinc(II), the d^{10} configuration of which is compatible with 4-, 5- or 6-coordinate geometries. The reaction of two equivalents of 2,2′-bipyridine-6-carbaldehyde with one equivalent each of (1*R*,2*R*)-(–)-1,2-diaminocyclohexane and $Zn(OAc)_2{\cdot}2H_2O$ followed by anion exchange, resulted in the formation of a white solid. In the FAB mass spectrum, the highest mass peaks at *m*/*z* 1457.3 and 1312.0 were consistent with $[Zn_2(\mathbf{4})_2(PF_6)_3]^+$ and $[Zn_2(\mathbf{4})_2(PF_6)_2]^+$ and the isotope patterns matched those simulated. The electrospray mass spectrum of a methanol solution of the complex showed only peaks for mononuclear species, and was dominated by peaks at *m*/*z* 719.3, 469.3 and 255.1 assigned to the ions $[Zn(\mathbf{4})PF_6 + 2MeOH]^+$, $[Na(\mathbf{4})]^+$ and $[Zn(\mathbf{4})]^{2+}$. The observed isotope patterns were consistent with those calculated. Although the mass spectrometric data were inconclusive as regards the nuclearity of the complex, the ^1H NMR spectrum of an MeCN solution of product showed that one of the cyclohexanedyl protons was significantly shielded (δ = –0.17 ppm). This mimics the scenario in $[Fe_2\{(S,S)\text{-}\mathbf{4}\}_2][PF_6]_4$ and $[Fe_2\{(R,R)\text{-}\mathbf{4}\}_2][PF_6]_4$, and suggested the presence of a double helicate in solution. This was confirmed for the solid state by single-crystal X-ray diffraction (see below). The ^1H and ^{13}C NMR spectra were

consistent with one ligand environment, and one diastereoisomer. In contrast to the ^{1}H NMR spectra of $[Fe_2\{(S,S)\text{-}\mathbf{4}\}_2][PF_6]_4$ and $[Fe_2\{(R,R)\text{-}\mathbf{4}\}_2][PF_6]_4$ in which the signals for protons H^{B3}, H^{B4} and H^{B5} overlap (Figure 9), that of the zinc(II) complex shows the doublet for H^{B5} (δ = 8.36 ppm) to be well separated from the signals for H^{B3} and H^{B4} (overlapping at δ = 8.91 ppm). The electronic absorption and CD spectra are presented in Figure 7 and S3, respectively. The former exhibits intense bands in the UV region, arising from $\pi^*\leftarrow\pi$ transitions.

Crystals of $[Zn_2\{(R,R)\text{-}\mathbf{4}\}_2][PF_6]_4\cdot 3MeCN$ suitable for X-ray diffraction were grown by slow diffusion of Et_2O into a MeCN solution of the compound over a period of 4 days. Figure 10 depicts the double helical $[Zn_2\{(R,R)\text{-}\mathbf{4}\}_2]^{4+}$ cation and confirms *M*-chirality. Interestingly, the relationship between the handedness of the helix and the chirality of the ligand is the opposite to that found in the iron(II) complex. Factors that appear to be associated with this difference are the coordination environment about the metal centre, and the orientation of the cyclohexanedyl units with respect to the M···M axis. In *M*-$[Fe_2\{(S,S)\text{-}\mathbf{4}\}_2]^{4+}$, each Fe^{II} centre is octahedrally sited with Fe–N bond lengths in the range 1.869(2)–1.985(2) Å. In *M*-$[Zn_2\{(R,R)\text{-}\mathbf{4}\}_2]^{4+}$, the six-coordinate geometry is appreciably distorted from regular octahedral with a rather large range of Zn–N bond lengths: 2.0406(19) to 2.3802(19) Å for Zn1 and 2.0357(19) to 2.356(2) Å for Zn2. The two longest contacts are to imine nitrogen donors. Figure 6 reveals that the imine-substituted C–C bond of each cyclohexanedyl unit is oriented parallel to the Fe···Fe axis. However, in *M*-$[Zn_2\{(R,R)\text{-}\mathbf{4}\}_2]^{4+}$, the imine-substituted C–C bonds are close to orthogonal with respect to the Zn···Zn axis. As a result, the Zn···Zn separation of 4.9698(8) Å is shorter than the Fe···Fe distance [5.2898(12) Å]. Just as in *M*-$[Fe_2\{(S,S)\text{-}\mathbf{4}\}_2][PF_6]_4$, the two imine units in *M*-$[Zn_2\{(R,R)\text{-}\mathbf{4}\}_2][PF_6]_4\cdot 3MeCN$ lie over one another (separation ca. 3.4 Å), and there is no intra- or inter-cation π-stacking between pyridine rings. The dominant packing forces involve C–H···F and C–H···N close contacts.

Although the detailed geometry of the double helicate in *M*-$[Zn_2\{(R,R)\text{-}\mathbf{4}\}_2]^{4+}$ is different from that in *M*-$[Fe_2\{(S,S)\text{-}\mathbf{4}\}_2]^{4+}$, each proton $H^{C3'}$ is still directed towards a pyridine π-cloud (Figure S4). In the solid state, the four $H^{C3'}$ protons are crystallographically inequivalent, but as Figure S4 shows, only a small perturbation of the ligands is required to render them equivalent in solution (and similarly for all other sets of four protons).

On going from *M*-$[Fe_2\{(S,S)\text{-}\mathbf{4}\}_2]^{4+}$ to *M*-$[Zn_2\{(R,R)\text{-}\mathbf{4}\}_2]^{4+}$, the coordination environment around the metal ion changes from octahedral to distorted octahedral, the latter tending towards five-coordinate. We therefore decided to investigate the consequences of introducing a metal ion for which a lower coordination number is typically preferred. The reaction of (1*R*,2*R*)-(–)-1,2-diaminocyclohexane with two equivalents of 2,2′-bipyridine-6-carbaldehyde and one equivalent of $AgBF_4$ yielded a yellow crystalline complex, for which X-ray quality crystals could be selected from the bulk sample. The highest mass peak envelope in the FAB mass spectrum came at *m*/*z* 1193.5 and was assigned to $[Ag_2(\mathbf{4})_2BF_4]^+$. The same ion was observed in the ESI mass spectrum of a methanol solution of the complex. In both spectra, the base peak corresponded to $[Ag(\mathbf{4})]^+$, with the characteristic isotope pattern of one silver. The formation of a double helicate was confirmed by single-crystal X-ray diffraction and the structure of the *M*-$[Ag_2\{(R,R)\text{-}\mathbf{4}\}_2]^{4+}$ cation in $2[Ag_2\{(R,R)\text{-}\mathbf{4}\}_2][BF_4]_2\cdot 3H_2O$ is presented in Figure 11. The bpy unit containing atoms N5 and N6 is disordered and has been modelled over two positions. In the second ligand, the portion from atom N9 through to the pyridine ring containing atom N12 is also disordered and has again been modelled over two positions. Each silver atom is bound by five nitrogen donors in a distorted coordination environment. The terminal pyridine donors are too distant from the metal centre for the Ag···N interactions to be considered important [Ag1···N12′ 3.439(10), Ag2···N6′ 3.166(11) Å]. Although the two ligands define an *M*-double helix, their arrangement around the dimetal core is distinct from those in *M*-$[Zn_2\{(R,R)\text{-}\mathbf{4}\}_2]^{4+}$ and *M*-$[Fe_2\{(S,S)\text{-}\mathbf{4}\}_2]^{4+}$. In $[Ag_2\{(R,R)\text{-}\mathbf{4}\}_2]^{2+}$, the Ag···Ag separation is 3.2223(8) Å, less than the sum of the van der Waals radii (3.44 Å), but at the longer end of what might be considered a metallophilic interaction.[44] Nonetheless, this interaction may be sufficient to control the organization of the two ligands and is similar to the distances of 3.107(2) Å[45] and 3.230(2) Å[46] in $[Ag_2(qtpy)_2]^{2+}$ and a chiral derivative thereof, respectively, (qtpy = 2,2′:6′,2″:6″,2‴-quaterpyridine), 2.9452(4) Å in $[Ag_2(Phtpy)_2]^{2+}$[47] and 2.8441(7) and 2.8955(6) Å within the two double helices in $[\{Ag_2(Phtpy)_2\}_2]^{4+}$[48] (Phtpy = 4′-phenyl-2,2′:6′,2″-terpyridine).

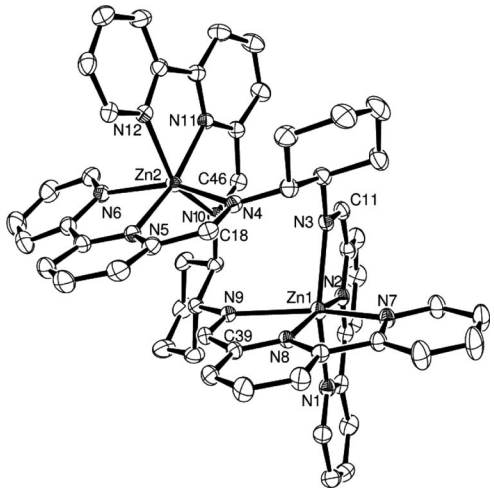

Figure 10. Structure of the *M*-$[Zn_2\{(R,R)\text{-}\mathbf{4}\}_2]^{4+}$ cation in *M*-$[Zn_2\{(R,R)\text{-}\mathbf{4}\}_2][PF_6]_4\cdot 3MeCN$ (ellipsoids plotted at the 40% probability level); H atoms omitted for clarity. Bond parameters in the coordination spheres: Zn1–N2 2.0406(19), Zn1–N8 2.0421(17), Zn1–N7 2.1546(19), Zn1–N1 2.240(2), Zn1–N3 2.297(2), Zn1–N9 2.3802(19), Zn2–N5 2.0357(19), Zn2–N11 2.0447(19), Zn2–N6 2.1904(19), Zn2–N10 2.2262(18), Zn2–N12 2.2589(19), Zn2–N4 2.356(2) Å; N2–Zn1–N1 74.81(8), N2–Zn1–N3 76.25(8), N8–Zn1–N7 76.83(7), N8–Zn1–N9 74.34(7), N5–Zn2–N4 75.54(7), N5–Zn2–N6 76.42(8), N11–Zn2–N10 76.74(7), N11–Zn2–N12 74.61(7)°.

Notably, the distance between the silver atoms in $[Ag_2\{(R,R)\text{-}\mathbf{4}\}_2]^{2+}$ is congruent with π-stacking between bpy domains, and the rings containing atoms N2 and N8 engage in a face-to-face interaction at a separation of 3.4 Å. The consequence of the latter structural feature is that the double helix is compressed with respect to those in *M*-$[Fe_2\{(S,S)\text{-}\mathbf{4}\}_2]^{4+}$ and *M*-$[Zn_2\{(R,R)\text{-}\mathbf{4}\}_2]^{4+}$, and the disilver helicate lacks the pseudo-symmetry possessed by the diiron (see insert in Figure 9) and dizinc species.

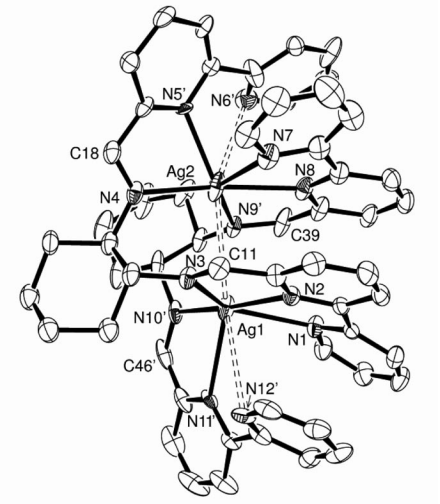

Figure 11. Structure of the *M*-$[Ag_2\{(R,R)\text{-}\mathbf{4}\}_2]^{2+}$ cation in $2[Ag_2\{(R,R)\text{-}\mathbf{4}\}_2][BF_4]_2{\cdot}3H_2O$ (ellipsoids plotted at the 30% probability level); for each disordered atom, one of two possible positions is shown. Hydrogen atoms are omitted for clarity. Selected bond parameters: Ag1–N1 2.577(3), Ag1–N2 2.382(3), Ag1–N3 2.375(3), Ag1–N10′ 2.357(10), Ag1–N11′ 2.594(12), Ag2–N4 2.275(3), Ag2–N5′ 2.240(10), Ag2–N7 2.599(4), Ag2–N8 2.357(3), Ag2–N9′ 2.491(11) Å; N2–Ag1–N1 65.04(11), N3–Ag1–N2 69.59(11), N10–Ag1–N3 117.4(2), N3–Ag1–N11′ 118.1(3), N1–Ag1–N11′ 83.9(3), N8–Ag2–N7 65.59(13), N5′–Ag2–N4 70.4(3), N8–Ag2–N9′ 72.7(3), N4–Ag2–N9′ 117.7(3), N5′–Ag2–N9′ 127.0(4)°.

Figure 11 reveals that, while the two ligand environments are similar in the *M*-$[Ag_2\{(R,R)\text{-}\mathbf{4}\}_2]^{2+}$ cation, the two bpy domains of a given ligand are distinct. However, the ^1H and ^{13}C NMR solution spectra (assigned by 2D-methods) are evidence for one ligand environment in which the bpy units are equivalent. The CD_3CN solution ^1H NMR spectrum of the silver(I)-containing product (Figure 12) shows notable differences when compared to those of the iron(II) (Figure 9) and zinc(II) complexes. Of particular note are the following. Whereas the signal for cyclohexanedyl proton $H^{C3'}$ appears at δ = –0.49 and –0.17 ppm in *M*-$[Fe_2\{(S,S)\text{-}\mathbf{4}\}_2][PF_6]_4$ and *M*-$[Zn_2\{(R,R)\text{-}\mathbf{4}\}_2][PF_6]_4$, respectively, it is observed at δ +1.89 ppm in $[Ag_2\{(R,R)\text{-}\mathbf{4}\}_2][BF_4]_2$. Secondly, the chemical shift of the signal for H^{A6} in the disilver complex compared with those in the diiron and dizinc complexes suggests that it does not lie over a pyridine π-cloud; this is consistent with the terminal pyridine ring (ring A, Scheme 1) in the silver complex being non-coordinated. Thirdly, the signal for the imine proton appears at higher frequency in the silver complex (δ 8.53 ppm) than in the iron (δ 8.02 ppm) or zinc (δ 8.07 ppm) double helicates (compare Figures 12 and 9), suggesting that the N=CH group in the former complex is not sandwiched in the middle of a helicate as in the latter two. Low temperature ^1H NMR spectra were recorded down to 235 K provided no information about possible dynamic processes because of the low solubilty of the complex at low temperatures. Although it is not possible to draw an unambiguous conclusion, the ^1H NMR spectroscopic data suggest that the double helical structure of $[Ag_2\{(R,R)\text{-}\mathbf{4}\}_2]^{2+}$ is not preserved in solution. It is significant, therefore, that the dominant peak in the ESI mass spectrum arises from the $[Ag(\mathbf{4})]^+$ ion (see above). The solution electronic absorption spectrum of $[Ag_2\{(R,R)\text{-}\mathbf{4}\}_2][BF_4]_2$ (Figure 7) exhibits the expected intense bands in the UV region, assigned to ligand-based π*←π transitions.

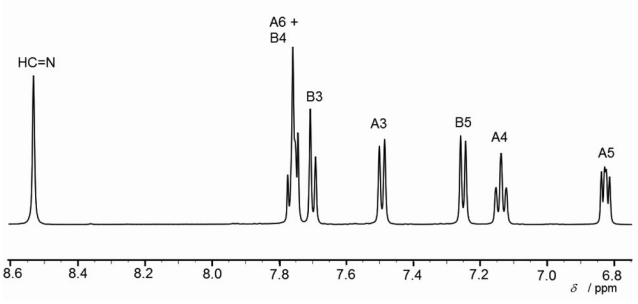

Figure 12. Part of the 500 MHz ^1H NMR spectrum of $[Ag_2\{(R,R)\text{-}\mathbf{4}\}_2][BF_4]_2$ in CD_3CN at room temperature. Atom labelling is given in Scheme 1.

Conclusions

Diamine–aldehyde condensation starting from an enantiopure diamine provides a facile way of accessing enantiopure hexadentate ligands as illustrated by the syntheses of (*R*,*R*)-**3**, (*R*,*R*)-**4** and (*S*,*S*)-**4**. Each tridentate metal-binding domain in (*R*,*R*)-**3** is quite flexible because of inversion at the amine nitrogen centre and rotation about the single bonds in the saturated spacers. This allows the formation of either *M*-$[M\{(R,R)\text{-}\mathbf{3}\}]^{2+}$ {in which each metal-bound amine nitrogen has an (*S*)-configuration} or *P*-$[M\{(R,R)\text{-}\mathbf{3}\}]^{2+}$ {in which the amine nitrogen has an (*R*)-configuration}. The solid-state structures of the copper(II), iron(II) and zinc(II) complexes each contain *M*-$[M\{(R,R)\text{-}\mathbf{3}\}]^{2+}$, while in solution, $[Fe\{(R,R)\text{-}\mathbf{3}\}]^{2+}$ exists predominantly as one diastereoisomer (assumed to be the *M*-form) with the proportion of the minor diastereoisomer being gradually diminished by successive recrystallizations. The preference for the *M*- over *P*-form can be rationalized in terms of a favourable *anti*-configuration of the NH and H^{C2} (Scheme 1) hydrogen atoms in the former, and an unfavourable *syn*-configuration in the latter. On going from (*R*,*R*)-**3** to the hexadentate Schiff bases (*R*,*R*)-**4** and (*S*,*S*)-**4**, the flexibility of the ligand backbone is reduced. These ligands bind iron(II), zinc(II) or silver(I) ions to give [2+2] double helicates, and complete stereochemical control has been

confirmed in the solid-state structures. In each of $[Fe_2\{(S,S)\text{-}\mathbf{4}\}_2]^{4+}$, $[Zn_2\{(R,R)\text{-}\mathbf{4}\}_2]^{4+}$ and $[Ag_2\{(R,R)\text{-}\mathbf{4}\}_2]^{2+}$, preference for an *M*-helicate is observed.

Experimental Section

General: ^1H and ^{13}C NMR spectra were recorded on Bruker DRX-500 or DPX-400 MHz spectrometers; chemical shifts for ^1H and ^{13}C NMR spectra are referenced to residual solvent peaks with respect to δ(TMS) = 0 ppm. Infrared spectra were recorded on a Shimadzu FTIR-8400S spectrophotometer with solid samples on a Golden Gate diamond ATR accessory. Solution electronic absorption spectra were recorded on a Varian-Cary 5000 spectrophotometer. Electrospray mass spectra were recorded using a Finnigan MAT LCQ mass spectrometer. The circular dichroism (CD) spectra were recorded on a DS62 spectropolarimeter (Aviv Associates, Lakewood, NJ) using Chirascan software (Applied Biophysics Ltd., Leatherhead, UK).

Commercially available enantiopure (1*R*,2*R*)-(–)- and (1*S*,2*S*)-(+)-1,2-diaminocyclohexane (Fluka) were reagent grade and used without further purification. 2,2′-Bipyridine-6-carbaldehyde was prepared according to a published procedure.[49]

(*R*,*R*)-3: 2,2′-Bipyridine-6-carbaldehyde (0.368 g, 2.00 mmol) was dissolved in MeOH (20 cm^3) and a solution of (1*R*,2*R*)-(–)-1,2-diaminocyclohexane (0.114 g, 1.00 mmol) in MeOH (10 cm^3) was added dropwise while the reaction mixture was stirred at room temperature. The resulting mixture was heated at reflux for 1 h, then allowed to cool to room temperature. Solid $NaBH_4$ (0.19 g, 5.0 mmol) was added in small portions over a period of 1 h, and the resulting colourless solution was stirred at room temperature overnight. The reaction was then quenched with saturated aqueous $NaHCO_3$. The mixture was extracted with $CHCl_3$ (3×30 cm^3), washed with water and brine, and dried with anhydrous Na_2SO_4. After filtration, the filtrate was evaporated to dryness. The crude product was purified by column chromatography (SiO_2, CH_2Cl_2/MeOH, v/v 3:1) and (*R*,*R*)-**3** was isolated as a colourless sticky oil (0.290 g, 0.644 mmol, 64.4%). ^1H NMR (500 MHz, $CDCl_3$): δ = 8.60 (d, *J* = 4.2 Hz, 2 H, H^{A6}), 8.32 (d, *J* = 7.9 Hz, 2 H, H^{A3}), 8.23 (d, *J* = 7.8 Hz, 2 H, H^{B3}), 7.69 (t, *J* = 7.7 Hz, 2 H, H^{B4}), 7.56 (t, *J* = 7.0 Hz, 2 H, H^{A4}), 7.33 (d, *J* = 7.6 Hz, 2 H, H^{B5}), 7.19 (m, 2 H, H^{A5}), 4.16 (d, *J* = 14.4 Hz, 2 H, H^{a}), 3.96 (d, *J* = 14.4 Hz, 2 H, $H^{a'}$), 3.10 (v br, 2 H, H^{NH}), 2.47 (m, 2 H, H^{C2}), 2.18 (m, 2 H, H^{C3}), 1.73 (m, 2 H, H^{C4}), 1.24 (m, 4 H, $H^{C3'+C4'}$) ppm. ^{13}C NMR (126 MHz, $CDCl_3$): δ = 158.8 (C^{B6}), 156.2 (C^{A2}), 155.7 (C^{B2}), 149.3 (C^{A6}), 137.6 (C^{B4}), 137.0 (C^{A4}), 123.8 (C^{A5}), 122.5 (C^{B5}), 121.3 (C^{A3}), 119.5 (C^{B3}), 61.3 (C^{C2}), 51.9 (C^{a}), 31.4 (C^{C3}), 25.1 (C^{C4}) ppm. IR (neat): $\tilde{\nu}$ = 2925 (m), 2853 (w), 1574 (s), 1560 (s), 1452 (m), 1427 (s), 1259 (w), 1145 (w), 1117 (w), 1094 (m), 1043 (m), 990 (m), 819 (w), 771 (s), 619 (m) cm^{-1}. UV/Vis (5.0×10^{-5} mol dm^{-3}, MeCN): λ_{max} (ε) = 239 (1.6), 281 nm (2.0×10^4 dm^3 mol^{-1} cm^{-1}). ESI-MS (MeOH): *m*/*z* = 451.5 $[M + H]^+$ (calcd. 451.3), 473.3 $[M + Na]^+$ (base peak, calcd. 473.2). $C_{28}H_{30}N_6 \cdot 1.2CH_2Cl_2$ (552.50): calcd. C 63.48, H 5.91, N 15.21; found C 63.55, H 5.91, N 15.80. $[\alpha]_D^{20}$ = –77.8 (*c* = 0.133, CH_2Cl_2).

[Zn{(*R*,*R*)-3}][PF$_6$]$_2$: $Zn(OAc)_2 \cdot 1.5H_2O$ (20.9 mg, 0.100 mmol) was added to a stirred solution of (*R*,*R*)-**3** (22.5 mg, 0.0500 mmol) in MeOH (5 cm^3) at room temperature. The colourless solution was stirred for 1 h, and then excess aqueous NH_4PF_6 (5 cm^3) was added dropwise. The white precipitate was collected by filtration and washed with H_2O and a few drops of MeOH. The product was redissolved in MeCN, then filtered and the filtrate was evaporated to dryness under reduced pressure to give $[Zn\{(R,R)\text{-}\mathbf{3}\}][PF_6]_2$ as a white solid (31.5 mg, 0.0391 mmol, 78.2%). ^1H NMR (500 MHz, CD_3CN): δ = 8.47 (d, *J* = 7.7 Hz, 2 H, $H^{B3/A3}$), 8.46 (d, *J* = 7.9 Hz, 2 H, $H^{B3/A3}$), 8.39 (t, *J* = 7.8 Hz, 2 H, H^{B4}), 8.15 (t, *J* = 7.8 Hz, 2 H, H^{A4}), 7.81 (d, *J* = 7.7 Hz, 2 H, H^{B5}), 7.72 (d, *J* = 4.9 Hz, 2 H, H^{A6}), 7.44 (m, 2 H, H^{A5}), 4.31 (d, *J* = 17.3 Hz, 2 H, H^{a}), 4.14 (dd, *J* = 5.7, 17.3 Hz, 2 H, $H^{a'}$), 2.94 (dd, *J* = 10.5, 5.9 Hz, 2 H, H^{NH}), 2.34 (d, *J* = 13.0 Hz, 2 H, H^{C3}), 2.01 (dt, *J* = 7.8, 21.0 Hz, 2 H, H^{C2}), 1.72 (m, 2 H, H^{C4}), 1.16 (dt, *J* = 10.8, 21.1 Hz, 2 H, $H^{C4'}$), 0.95 (m, 2 H, $H^{C3'}$) ppm. ^{13}C NMR (126 MHz, CD_3CN): δ = 157.2 (C^{B6}), 149.8 ($C^{A2/B2}$), 149.7 ($C^{B2/A2}$), 149.5 (C^{A6}), 144.1 (C^{B4}), 142.6 (C^{A4}), 128.4 (C^{A5}), 127.6 (C^{B5}), 123.7 ($C^{A3/B3}$), 122.3 ($C^{B3/A3}$), 61.4 (C^{C2}), 48.0 (C^{a}), 31.7 (C^{C3}), 25.8 (C^{C4}) ppm. IR (solid): $\tilde{\nu}$ = 2931 (w), 2863 (w), 1600 (m), 1583 (w), 1454 (m), 1309 (w), 1254 (w), 1163 (w), 1094 (w), 1028 (w), 944 (w), 881 (m), 829 (s), 770 (s), 662 (m), 633 (m) cm^{-1}. UV/Vis (5.0×10^{-5} mol dm^{-3}, MeCN): λ_{max} (ε) = 247 (1.8), 299 (2.6), 311 nm (2.6×10^4 dm^3 mol^{-1} cm^{-1}). ESI-MS (MeOH): *m*/*z* = 659.6 $[M - PF_6]^+$ (base peak, calcd. 659.2), 257.4 $[M - 2PF_6]^{2+}$ (calcd. 257.1). $C_{28}H_{30}F_{12}N_6P_2Zn$ (805.92): calcd. C 41.73, H 3.75, N 10.43; found C 40.91, H 3.87, N 10.11.

[Cu{(*R*,*R*)-3}][PF$_6$]$_2$: Anhydrous $Cu(OAc)_2$ (18.1 mg, 0.100 mmol) was added to a stirred solution of (*R*,*R*)-**3** (22.5 mg, 0.0500 mmol) in MeOH (5 cm^3) at room temperature. The blue solution was stirred for 1 h, then excess aqueous NH_4PF_6 (5 cm^3) was added dropwise. The reaction mixture was stirred for 30 min, then left to stand at room temperature to allow the solvent to evaporate. Blue needle-like microcrystals formed within 2 d. The solid was collected by filtration, washed with H_2O and dried in vacuo. $[Cu\{(R,R)\text{-}\mathbf{3}\}][PF_6]_2$ was isolated as a blue crystalline solid (23.0 mg, 0.0286 mmol, 57.2%). IR (solid): $\tilde{\nu}$ = 2934 (w), 2867 (w), 1600 (m), 1580 (w), 1456 (m), 1434 (w), 1299 (w), 1251 (w), 1182 (w), 1096 (w), 1030 (w), 828 (s), 773 (s), 661 (w), 633 (w) cm^{-1}. UV/Vis (5.0×10^{-5} mol dm^{-3}, MeCN): λ_{max} (ε) = 229 (2.2), 299 (2.4), 310 sh nm (2.1×10^4 dm^3 mol^{-1} cm^{-1}). ESI-MS (MeOH): *m*/*z* = 658.3 $[M - PF_6]^+$ (base peak, calcd. 658.2), 256.8 $[M - 2PF_6]^{2+}$ (calcd. 256.6). $C_{28}H_{30}CuF_{12}N_6P_2 \cdot 2H_2O$ (840.08): calcd. C 40.03, H 4.08, N 9.93; found C 39.61, H 3.83, N 9.93.

[Fe{(*R*,*R*)-3}][BF$_4$]$_2$: $Fe(BF_4)_2 \cdot 6H_2O$ (16.9 mg, 0.0500 mmol) was added to a stirred solution of (*R*,*R*)-**3** (22.5 mg, 0.0500 mmol) in MeCN (10 cm^3) at room temperature. After being stirred for 1 h, the dark-brown solution was filtered, and the filtrate was evaporated to dryness under reduced pressure. The resulting deep-purple solid was washed well with Et_2O and was dried in vacuo over P_2O_5. $[Fe\{(R,R)\text{-}\mathbf{3}\}][BF_4]_2$ was isolated as a black-purple solid (31.3 mg, 0.0460 mmol, 92.0%). ^1H NMR (500 MHz, CD_3CN): δ = 8.77 (d, *J* = 8.0 Hz, 2 H, H^{B3}), 8.53 (d, *J* = 8.0 Hz, 2 H, H^{A3}), 8.33 (t, *J* = 7.9 Hz, 2 H, H^{B4}), 8.00 (d, *J* = 7.8 Hz, 2 H, H^{B5}), 7.91 (t, *J* = 7.7 Hz, 2 H, H^{A4}), 7.13 (m, 2 H, H^{A5}), 6.82 (d, *J* = 5.5 Hz, 2 H, H^{A6}), 4.34 (d, *J* = 16.5 Hz, 2 H, H^{a}), 3.38 (dd, *J* = 16.1, 3.2 Hz, 2 H, $H^{a'}$), 2.79 (s, 2 H, H^{NH}), 2.21 (d, *J* = 12.8 Hz, 2 H, H^{C3}), 1.73 (m, 2 H, H^{C2}), 1.60 (d, *J* = 9.0 Hz, 2 H, H^{C4}), 1.01 (m, 2 H, $H^{C4'}$), 0.86 (m, 2 H, $H^{C3'}$) ppm. ^{13}C NMR (126 MHz, CD_3CN): δ = 165.8 (C^{B6}), 161.7 (C^{A2+B2}), 155.3 (C^{A6}), 138.6 (C^{A4}), 137.8 (C^{B4}), 127.4 (C^{A5}), 124.9 (C^{B5}), 124.5 (C^{A3}), 123.5 (C^{B3}), 66.9 (C^{C2}), 56.3 (C^{a}), 30.6 (C^{C3}), 25.5 (C^{C4}) ppm. IR (solid): $\tilde{\nu}$ = 2937 (w), 2863 (w), 1606 (m), 1453 (s), 1408 (s), 1286 (w), 1031 (s), 1001 (s), 882 (w), 839 (m), 772 (s), 664 (w) cm^{-1}. UV/Vis (5.0×10^{-5} mol dm^{-3}, MeCN): λ_{max} (ε) 247 (1.9), 302 (3.3), 373 (0.35), 578 nm (0.45×10^4 dm^3 mol^{-1} cm^{-1}). ESI-MS (MeOH): *m*/*z* = 593.0 $[M - PF_6]^+$ (calcd. 593.2), 253.1 $[M - 2PF_6]^{2+}$ (base peak, calcd. 253.1). $C_{28}H_{30}B_2F_8FeN_6 \cdot 4H_2O$ (752.09): calcd. C 44.72, H 5.09, N 11.17; found C 44.24, H 4.31, N 10.96.

$[Fe_2\{(S,S)\text{-}4\}_2][PF_6]_4$: (1*S*,2*S*)-(+)-1,2-Diaminocyclohexane (11.4 mg, 0.100 mmol) and 2,2′-bipyridine-6-carbaldehyde (36.8 mg, 0.200 mmol) were dissolved in MeOH (3 cm^3). Solid $FeCl_2{\cdot}4H_2O$ (19.8 mg, 0.100 mmol) was added to the stirred solution at room temperature, and the resulting deep-violet solution was stirrd for 1 h. Aqueous NH_4PF_6 (163 mg, 1.00 mmol in 8 cm^3 H_2O) was added dropwise while the reaction mixture was stirred and a purple precipitate formed. The resulting suspension was allowed to stand for 1 h, after which time it was filtered by suction, and washed with MeOH/H_2O (3.0 cm^3, v/v, 1:5). The resulting purple solid was redissolved in MeCN, filtered and solvent was then removed under vacuum. The product was dried in vacuo over P_2O_5. $[Fe_2\{(S,S)\text{-}4\}_2][PF_6]_4$ was isolated as a purple powder (60.2 mg, 76.0%). ^{1}H NMR (500 MHz, CD_3CN): δ = 8.90 (dd, J = 7.3, 1.8 Hz, 2 H, H^{B3}), 8.87 (m, 4 H, H^{B4+B5}), 8.42 (d, J = 7.9 Hz, 2 H, H^{A3}), 8.02 (s, 2 H, H^a), 7.94 (dt, J = 7.8, 1.3 Hz, 2 H, H^{A4}), 7.13 (m, 2 H, H^{A5}), 6.69 (d, J = 5.6 Hz, 2 H, H^{A6}), 2.20 (m, 2 H, H^{C2}), 0.98 (d, J = 8.4 Hz, 2 H, $H^{C4'}$), 0.63 (m, 2 H, H^{C3}), 0.58 (d, J = 10.6 Hz, 2 H, H^{C4}), –0.49 (d, J = 12.6 Hz, 2 H, $H^{C3'}$) ppm. ^{13}C NMR (126 MHz, $CDCl_3$): δ = 170.9 (C^a), 161.3 (C^{B2}), 159.3 (C^{B6}), 157.5 (C^{A2}), 153.9 (C^{A6}), 141.2 ($C^{B4/B5}$), 140.5 (C^{A4}), 130.6 ($C^{B5/B4}$), 129.6 (C^{A5}), 125.4 (C^{B3}), 125.0 (C^{A3}), 69.8 (C^{C2}), 37.2 (C^{C3}), 24.3 (C^{C4}) ppm. IR (neat): $\tilde{\nu}$ = 1739 (w), 1607 (w), 1455 (m), 1400 (w), 1373 (w), 1290 (w), 1230 (w), 834 (s), 765 (s), 739 (s), 669 (m) cm^{-1}. UV/Vis (2.5×10^{-5} mol dm^{-3}, MeCN): λ_{max} (ε) = 229 (8.2), 268 (6.0), 322 (4.6), 341sh (2.7), 484 (1.1), 604 (1.3), 710sh nm (0.19×10^4 $dm^3\,mol^{-1}\,cm^{-1}$). ESI-MS (MeOH) m/z = 647.1 [M – $2PF_6$]$^{2+}$ (calcd. 647.1), 521.2 [Fe(**4**) + F]$^+$ (calcd. 521.2), 501.2 [Na(**4**) + MeOH]$^+$ (calcd. 501.2), 469.2 [Na(**4**)]$^+$ (calcd. 469.2), 251.1 [Fe(**4**)]$^{2+}$ (calcd. 251.1). FAB-MS m/z = 1439.3 [M – PF_6]$^+$ (calcd. 1439.3), 1293.8 [M – $2PF_6$]$^+$ (calcd. 1294.2), 1149.9 [M – $3PF_6$]$^+$ (calcd. 1149.3). $C_{56}H_{52}F_{24}Fe_2N_{12}P_4{\cdot}2.5H_2O$ (1629.68): calcd. C 41.27, H 3.53, N 10.31; found C 40.91, H 3.62, N 10.47.

$[Fe_2\{(R,R)\text{-}4\}_2][PF_6]_4$: The complex was prepared in the same manner as $[Fe_2\{(S,S)\text{-}4\}_2][PF_6]_4$ starting with (1*R*,2*R*)-(–)-1,2-diaminocyclohexane (11.4 mg, 0.100 mmol), 2,2′-bipyridine-6-carbaldehyde (36.8 mg, 0.200 mmol) and $FeCl_2{\cdot}4H_2O$ (19.8 mg, 0.100 mmol). $[Fe_2\{(R,R)\text{-}4\}_2][PF_6]_4$ was isolated as purple microcrystals (62.9 mg, 79.4%). ^{1}H NMR spectroscopic data exactly matched those of $[Fe_2\{(S,S)\text{-}4\}_2][PF_6]_4$. $C_{56}H_{52}F_{24}Fe_2N_{12}P_4{\cdot}2.5H_2O$ (1629.68): calcd. C 41.27, H 3.53, N 10.31; found C 41.18, H 3.55, N 10.40.

$[Zn_2\{(R,R)\text{-}4\}_2][PF_6]_4$: The complex was prepared in the same manner as $[Fe_2\{(S,S)\text{-}4\}_2][PF_6]_4$ starting with (1*R*,2*R*)-(–)-1,2-diaminocyclohexane (11.4 mg, 0.100 mmol), 2,2′-bipyridine-6-carbaldehyde (36.8 mg, 0.200 mmol) and $Zn(OAc)_2{\cdot}2H_2O$ (21.8 mg, 0.100 mmol). $[Zn_2\{(R,R)\text{-}4\}_2][PF_6]_4$ was isolated as a white solid (64.0 mg, 80.0%). ^{1}H NMR (500 MHz, CD_3CN): δ = 8.91 (m, 4 H, H^{B3+B4}), 8.56 (d, J = 7.9 Hz, 2 H, H^{A3}), 8.36 (d, J = 6.9 Hz, 2 H, H^{B5}), 8.18 (dt, J = 7.8, 1.2 Hz, 2 H, H^{A4}), 8.07 (s, 2 H, H^a), 7.42 (m, 2 H, H^{A5}), 7.36 (d, J = 4.7 Hz, 2 H, H^{A6}), 2.55 (d, J = 9.7 Hz, 2 H, H^{C2}), 1.13 (m, 4 H, H^{C4}), 1.11 (m, 4 H, H^{C3}), 0.71 (d, J = 9.6 Hz, 2 H, $H^{C4'}$), –0.17 (s, 2 H, $H^{C3'}$) ppm. ^{13}C NMR (126 MHz, $CDCl_3$): δ = 165.0 (C^a), 151.1 (C^{B2}), 149.2 (C^{A6}), 147.4 (C^{B4}), 147.4 (C^{A2}), 145.9 (C^{B6}), 142.9 (C^{A4}), 131.5 (C^{B5}), 129.4 (C^{A5}), 128.6 (C^{B3}), 125.1 (C^{A3}), 72.2 (C^{C2}), 37.8 (C^{C3}), 24.8 (C^{C4}) ppm. IR (neat): $\tilde{\nu}$ = 1590 (m), 1490 (w), 1452 (m), 1324 (w), 1301 (w), 1257 (w), 1182 (w), 1164 (w), 1097 (w), 1030 (m), 1013 (w), 875 (m), 837 (s), 777 (m), 739 (w), 662 (m) cm^{-1}. UV/Vis (2.5×10^{-5} mol dm^{-3}, MeCN): λ_{max} (ε) = 229 (5.4), 247 (4.3), 276 (2.6), 299 (3.5), 311 (4.1), 331sh nm (2.1×10^4 $dm^3\,mol^{-1}\,cm^{-1}$). ESI-MS (MeOH) m/z = 719.3 [Zn(**4**)PF_6 + 2MeOH]$^+$ (calcd. 719.2), 469.3 [Na(**4**)]$^+$ (calcd. 469.2), 287.1 [Zn(**4**) + 2MeOH]$^{2+}$ (calcd. 287.1), 271.1 [Zn(**4**) + MeOH]$^{2+}$ (calcd. 271.1), 255.1 [Zn(**4**)]$^{2+}$ (calcd. 255.1). FAB-MS m/z = 1457.3 [M – PF_6]$^+$ (calcd. 1457.2), 1312.0 [M – $2PF_6$]$^+$ (calcd. 1312.2), 510.0 [Zn(**4**)]$^+$ (calcd. 510.2). $C_{56}H_{52}F_{24}N_{12}P_4Zn_2{\cdot}2MeOH{\cdot}H_2O$ (1685.87): calcd. C 41.32, H 3.71, N 9.97; found C 41.17, H 3.74, N 9.85.

$[Ag_2\{(R,R)\text{-}4\}_2][BF_4]_2$: (1*R*,2*R*)-(+)-1,2-Diaminocyclohexane (11.4 mg, 0.100 mmol) and 2,2′-bipyridine-6-carbaldehyde (36.8 mg, 0.200 mmol) were dissolved in MeOH (3.0 cm^3). The reaction mixture was stirred at room temperature while solid $AgBF_4$ (19.4 mg, 0.100 mmol) was added. The resulting light yellow solution was stirred for 2 h, after which time water (8.0 cm^3) was added. The resulting solution was allowed to stand in air and in the dark for two weeks. During this period, yellow blocks of $[Ag_2\{(R,R)\text{-}4\}_2][BF_4]_2$ formed. These were collected by filtration, washed with Et_2O and dried in air (25.2 mg, 39.4%). ^{1}H NMR (500 MHz, CD_3CN): δ = 8.53 (s, 2 H, H^a), 7.76 (m, 4 H, H^{B4+A6}), 7.70 (d, J = 7.9 Hz, 2 H, H^{B3}), 7.49 (d, J = 7.9 Hz, 2 H, H^{A3}), 7.25 (d, J = 7.5 Hz, 2 H, H^{B5}), 7.14 (t, J = 7.7 Hz, 2 H, H^{A5}), 6.83 (dd, J = 4.9, 7.3 Hz, 2 H, H^{A4}), 3.98 (d, J = 9.1 Hz, 2 H, H^{C2}), 2.09 (m, 2 H, H^{C3}), 1.89 (m, 4 H, $H^{C4+C3'}$), 1.47 (m, 2 H, $H^{C4'}$) ppm. ^{13}C NMR (126 MHz, $CDCl_3$): δ = 161.8 (C^a), 154.6 (C^{B2}), 153.2 (C^{A2}), 149.8 (C^{B6}), 149.1 (C^{A6}), 140.0 (C^{B4}), 137.3 (C^{A4}), 128.2 (C^{B5}), 125.7 (C^{B3}), 125.3 (C^{A5}), 122.5 (C^{A3}), 72.7 (C^{C2}), 33.1 (C^{C3}), 25.3 (C^{C4}) ppm. IR (neat): $\tilde{\nu}$ = 3590 (w), 2930 (w), 1643 (m), 1582 (m), 1562 (m), 1481 (w), 1447 (m), 1431 (m), 1391 (w), 1346 (w), 1308 (w), 1285 (w), 1250 (w), 1157 (w), 1051 (s), 1005 (s), 939 (w), 856 (w), 827 (w), 775 (s), 743 (m), 686 (w) cm^{-1}. UV/Vis (2.5×10^{-5} mol dm^{-3}, MeCN): λ_{max} (ε) = 228 (7.5), 246sh (4.6), 278 nm (4.1×10^4 $dm^3\,mol^{-1}\,cm^{-1}$). ESI-MS (MeOH) m/z = 1193.5 [M – BF_4]$^+$ (calcd. 1193.3), 553.3 [Ag(**4**)]$^+$ (calcd. 553.1). FAB-MS m/z = 1195.1 [M – BF_4]$^+$ (calcd. 1193.3), 553.1 [Ag(**4**)]$^+$ (calcd. 553.1). $C_{56}H_{52}Ag_2B_2F_8N_{12}{\cdot}H_2O$ (1300.45): calcd. C 51.72, H 4.19, N 12.92; found C 51.52, H 4.30, N 12.88.

Crystal Structure Determinations: Data were collected on a Bruker–Nonius Kappa CCD or Stoe IPDS instrument; data reduction, solution and refinement used the programs COLLECT,[50] SIR92,[51] DENZO/SCALEPACK[52] and CRYSTALS,[53] or Stoe IPDS software[54] and SHELXL97.[55] Structures have been analyzed using Mercury v.2.2.[56] ORTEP figures were drawn using Ortep-3 for Windows.[57]

$[Zn\{(R,R)\text{-}3\}][PF_6]_2$: $C_{28}H_{30}F_{12}N_6P_2Zn$, M = 805.89, colourless needle, orthorhombic, space group $P2_12_12_1$, a = 12.4555(4), b = 13.8457(4), c = 18.3334(5) Å, U = 3161.7(2) Å^3, Z = 4, Dc = 1.693 Mg m^{-3}, μ(Mo-K_α) = 0.981 mm^{-1}, T = 123 K. Total 132107 reflections, 15364 unique, R_{int} = 0.028. Refinement of 12976 reflections (443 parameters) with $I > 2\sigma(I)$ converged at final $R1$ = 0.0233 ($R1$ all data: 0.0276), $wR2$ = 0.0273 ($wR2$ all data: 0.0344), gof = 0.9901, Flack: 0.008(3).

$[Cu\{(R,R)\text{-}3\}][PF_6]_2$: $C_{28}H_{30}CuF_{12}N_6P_2$, M = 804.06, blue-green prism, orthorhombic, space group $P2_12_12_1$, a = 12.3960(2), b = 13.8237(2), c = 18.4391(3) Å, U = 3159.70(9) Å^3, Z = 4, Dc = 1.690 Mg m^{-3}, μ(Mo-K_α) = 0.896 mm^{-1}, T = 123 K. Total 59380 reflections, 12483 unique, R_{int} = 0.034. Refinement of 10796 reflections (443 parameters) with $I > 2\sigma(I)$ converged at final $R1$ = 0.0241 ($R1$ all data: 0.0279), $wR2$ = 0.0269 ($wR2$ all data: 0.0327), gof = 1.0865, Flack: 0.003(4).

$[Fe\{(R,R)\text{-}3\}][BF_4]_2$: $C_{28}H_{30}B_2F_8FeN_6$, M = 680.05, black block, orthorhombic, space group $P2_12_12_1$, a = 10.349(2), b = 14.929(3), c = 18.622(4) Å, U = 2877.1(10) Å^3, Z = 4, Dc = 1.570 Mg m^{-3}, μ(Mo-K_α) = 0.608 mm^{-1}, T = 173(2) K. Total 50913 reflections, 8297 unique, R_{int} = 0.128. Refinement of 8210 reflections (406 parameters) with $I > 2\sigma(I)$ converged at final $R1$ = 0.0344 ($R1$ all

data: 0.0347), *wR*2 = 0.0936 (*wR*2 all data: 0.0939), gof = 1.057, Flack: 0.009(8).

4[Fe$_2${(*S*,*S*)-4**}$_2$][PF$_6$]$_4$·4Et$_2$O·6Me$_2$CO·7MeCN·4H$_2$O:** $C_{272}H_{313}F_{96}Fe_8N_{55}O_{14}P_{16}$, M = 7343.11, black block, orthorhombic, space group $P2_12_12$, a = 23.634(5), b = 24.750(5), c = 13.846(3) Å, U = 8099(3) Å^3, Z = 1, Dc = 1.504 Mg m^{-3}, μ(Mo-K_α) = 0.547 mm^{-1}, T = 173 K. Total 146112 reflections, 20476 unique, R_{int} = 0.0828. Refinement of 19838 reflections (1148 parameters) with $I > 2\sigma(I)$ converged at final $R1$ = 0.0488 ($R1$ all data: 0.0503), $wR2$ = 0.1313 ($wR2$ all data: 0.1328), gof = 1.049, Flack: 0.032(10).

[Zn$_2${(*R*,*R*)-4**}$_2$][PF$_6$]$_4$·3MeCN:** $C_{62}H_{61}F_{24}N_{15}P_4Zn_2$, M = 1726.92, colourless block, monoclinic, space group $P2_1$, a = 13.6123(14), b = 21.961(3), c = 13.5795(16) Å, β = 119.736(8)°, U = 3524.8(7) Å^3, Z = 2, Dc = 1.627 Mg m^{-3}, μ(Mo-K_α) = 0.887 mm^{-1}, T = 173 K. Total 56323 reflections, 19608 unique, R_{int} = 0.0448. Refinement of 18689 reflections (1078 parameters) with $I > 2\sigma(I)$ converged at final $R1$ = 0.0363 ($R1$ all data: 0.0391), $wR2$ = 0.0876 ($wR2$ all data: 0.0890), gof = 1.082, Flack: 0.025(4).

2[Ag$_2${(*R*,*R*)-4**}$_2$][BF$_4$]$_2$·3H$_2$O:** $C_{112}H_{110}Ag_4B_4F_{16}N_{24}O_3$, M = 2618.97, yellow block, monoclinic, space group $P2_1$, a = 13.312(3), b = 13.841(3), c = 15.421(3) Å, β = 96.80(3)°, U = 2821.5(10) Å^3, Z = 1, Dc = 1.538 Mg m^{-3}, μ(Mo-K_α) = 0.773 mm^{-1}, T = 173 K. Total 61381 reflections, 14640 unique, R_{int} = 0.0260. Refinement of 14368 reflections (1094 parameters) with $I > 2\sigma(I)$ converged at final $R1$ = 0.0464 ($R1$ all data: 0.0472), $wR2$ = 0.1146 ($wR2$ all data: 0.1154), gof = 1.062, Flack: 0.00(2).

CCDC-746854 (for [Cu{(*R*,*R*)-**3**}][PF$_6$]$_2$), -746855 (for [Fe{(*R*,*R*)-**3**}][BF$_4$]$_2$), -746856 (for [Zn{(*R*,*R*)-**3**}][PF$_6$]$_2$), -757510 (for [Zn$_2${(*R*,*R*)-**4**}$_2$][PF$_6$]$_4$·3MeCN), -757511 (for 4[Fe$_2${(*S*,*S*)-**4**}$_2$]-[PF$_6$]$_4$·4Et$_2$O·6Me$_2$CO·7MeCN·4H$_2$O), -757512 (for 2[Ag$_2${(*R*,*R*)-**4**}$_2$][BF$_4$]$_2$·3H$_2$O) contain the supplementary crystallographic data for this paper. These data can be obtained free of charge from The Cambridge Crystallographic Data Centre via www.ccdc.cam.ac.uk/data_request/cif.

Supporting Information (see also the footnote on the first page of this article): Figure S1. ^{1}H NMR spectrum of (*R*,*R*)-**3**; Figure S2. CD spectra of (*R*,*R*)-**3**, [Zn{(*R*,*R*)-**3**}][PF$_6$]$_2$, [Cu{(*R*,*R*)-**3**}][PF$_6$]$_2$ and [Fe{(*R*,*R*)-**3**}][BF$_4$]$_2$; Figure S3. CD spectrum of [Zn$_2${(*R*,*R*)-**4**}$_2$][PF$_6$]$_4$; Figure S4. Space filling diagram of *M*-[Zn$_2${(*R*,*R*)-**4**}$_2$]$^{4+}$.

Acknowledgments

We thank the Swiss National Science Foundation and the University of Basel for financial support. Kate Harris and Peter Kopecky are acknowledged for recording the 500 MHz NMR spectra.

[1] E. L. Eliel, S. H. Wilen, *Stereochemistry of Organic Compounds*, Wiley, New York, **1994**.
[2] H. Amouri, M. Gruselle, *Chirality in Transition Metal Chemistry*, Wiley, New York, **2009**; A. von Zelewsky, *Stereochemistry of Coordination Compounds*, Wiley-VCH, Weinheim, **1996**; U. Knof, A. von Zelewsky, *Angew. Chem. Int. Ed.* **1999**, *38*, 302–320.
[3] R. B. King, *Chirality* **2001**, *13*, 465–473.
[4] L. N. Essen, F. A. Zakharova, A. D. Gel'man, *Zh. Neorg. Khim.* **1958**, *3*, 2654–2661.
[5] L. N. Essen, A. D. Helman, *Dokl. Akad. Nauk SSSR* **1956**, *108*, 651–654.
[6] P. K. Baker, M. E. Harman, D. A. Kendrick, M. B. Hursthouse, *Inorg. Chem.* **1993**, *32*, 3395–3396.
[7] J. C. Bailar, *Coord. Chem. Rev.* **1990**, *100*, 1–27.
[8] A. von Zelewsky, *Stereochemistry of Coordination Compounds*, Wiley, Chichester, England, New York, **1996**.
[9] A. von Zelewsky, *Coord. Chem. Rev.* **1999**, *192*, 811–825.
[10] E. C. Constable, *Chirality – The Dark Lady of Inorganic Chemistry* in *Education in Advanced Chemistry*, *Perspectives in Coordination Chemistry* (Eds.: A. M. Trzeciak, P. Sobota, J. J. Ziolkowski), vol. 7, University Publishing House (Wydawnictwa Uniwersytetu Wroclawskiego), Poznan-Wroclaw, **2000**, pp. 159–184.
[11] C. R. K. Glasson, L. F. Lindoy, G. V. Meehan, *Coord. Chem. Rev.* **2008**, *252*, 940–963.
[12] N. C. Fletcher, *J. Chem. Soc. Perkin Trans. 1* **2002**, 1831–1842.
[13] G. Chelucci, R. P. Thummel, *Chem. Rev.* **2002**, *102*, 3129–3170.
[14] R. Prabaharan, R. E. Oakes, N. C. Fletcher, M. Nieuwenhuyzen, *Tetrahedron: Asymmetry* **2004**, *15*, 2527–2532.
[15] R. Prabaharan, N. C. Fletcher, *Dalton Trans.* **2003**, 2558–2563.
[16] L. E. Perret-Aebi, A. von Zelewsky, *Synlett* **2002**, 773–774.
[17] O. Mamula, A. von Zelewsky, P. Brodard, C. W. Schläpfer, G. Bernardinelli, H. Stoeckli-Evans, *Chem. Eur. J.* **2005**, *11*, 3049–3057.
[18] H. Weizman, J. Libman, A. Shanzer, *J. Am. Chem. Soc.* **1998**, *120*, 2188–2189.
[19] K. N. Raymond, E. A. Dertz, S. S. Kim, *Proc. Natl. Acad. Sci. USA* **2003**, *100*, 3584–3588.
[20] N. C. Fletcher, C. Martin, H. J. Abraham, *New J. Chem.* **2007**, *31*, 1407–1411.
[21] R. Annunziata, M. Benaglia, M. Cinquini, F. Cozzi, C. R. Woods, J. S. Siegel, *Eur. J. Org. Chem.* **2001**, 173–180.
[22] R. J. Warr, A. C. Willis, S. B. Wild, *Inorg. Chem.* **2006**, *45*, 8618–8627.
[23] R. J. Warr, A. C. Willis, S. B. Wild, *Inorg. Chem.* **2008**, *47*, 9351–9362.
[24] R. Noyori in *Stereocontrolled Organic Synthesis* (Ed.: B. M. Trost), Blackwell, London, **1994**, pp. 1–15.
[25] Y.-M. Li, F.-Y. Kwong, W.-Y. Yu, A. S. C. Chan, *Coord. Chem. Rev.* **2007**, *251*, 2119–2144.
[26] W. Zhang, Y. Chi, X. Zhang, *Acc. Chem. Res.* **2007**, *40*, 1278–1290.
[27] S. G. Telfer, R. Kuroda, *Coord. Chem. Rev.* **2003**, *242*, 33–46.
[28] J. Bunzen, T. Bruhn, G. Bringmann, A. Lützen, *J. Am. Chem. Soc.* **2009**, *131*, 3621–3630.
[29] T. Nabeshima, A. Hashiguchi, T. Saiki, S. Akine, *Angew. Chem. Int. Ed.* **2002**, *41*, 481–484.
[30] A. Lutzen, M. Hapke, J. Griep-Raming, D. Haase, W. Saak, *Angew. Chem. Int. Ed.* **2002**, *41*, 2086–2089.
[31] M. Kimura, M. Sano, T. Muto, K. Hanabusa, H. Shirai, N. Kobayashi, *Macromolecules* **1999**, *32*, 7951–7953.
[32] J. Hamblin, L. J. Childs, N. W. Alcock, M. J. Hannon, *J. Chem. Soc., Dalton Trans.* **2002**, 164–169.
[33] G. F. Zi, C. L. Yin, *J. Mol. Catal. A* **1998**, *132*, L1–L4.
[34] E. C. Constable, G. Zhang, C. E. Housecroft, M. Neuburger, S. Schaffner, *Dalton Trans.* **2009**, 8165–8167.
[35] M. J. Hannon, C. L. Painting, J. Hamblin, A. Jackson, W. Errington, *Chem. Commun.* **1997**, 1807–1808.
[36] See for example: C.-M. Che, J.-S. Huang, *Coord. Chem. Rev.* **2003**, *242*, 97–113; P. G. Cozzi, *Chem. Soc. Rev.* **2004**, *33*, 410–421; J. F. Larrow, E. N. Jacobsen, *Top. Organomet. Chem.* **2004**, *6*, 123–152.
[37] E. C. Constable, G. Zhang, C. E. Housecroft, M. Neuburger, S. Schaffner, W.-D. Woggon, *New J. Chem.* **2009**, *33*, 1064–1069.
[38] G. Zhang, E. Yashima, W.-D. Woggon, *Adv. Synth. Catal.* **2009**, *351*, 1255–1262.
[39] E. C. Constable, G. Zhang, C. E. Housecroft, M. Neuburger, S. Schaffner, W.-D. Woggon, J. A. Zampese, *New J. Chem.* **2009**, *33*, 2166–2173.
[40] S. Akine, T. Matsumoto, T. Nabeshima, *Chem. Commun.* **2008**, 4604–4606.
[41] K. Popper, 7. *Simplicity*, *The Logic of Scientific Discovery*, **1992**, 2nd ed., Routledge, London, pp. 121–132.

[42] *PM3 Spartan '08*, Version 1.1.1, B. J. Deppmeier, A. J. Driessen, et al., Wavefunction Inc. Irvine, CA.
[43] V. Amendola, L. Fabbrizzi, C. Mangano, P. Pallavicini, E. Roboli, M. Zema, *Inorg. Chem.* **2000**, *39*, 5803–5806.
[44] P. Pyykko, N. Runeberg, F. Mendizabel, *Chem. Eur. J.* **1997**, *3*, 1451–1457.
[45] E. C. Constable, S. M. Elder, M. J. Hannon, A. Martin, P. R. Raithby, D. A. Tocher, *J. Chem. Soc., Dalton Trans.* **1996**, 2423–2433.
[46] G. Baum, E. C. Constable, D. Fenske, C. E. Housecroft, T. Kulke, *Chem. Eur. J.* **1999**, *5*, 1862–1873.
[47] Z. Ma, Y. Xing, M. Yang, M. Hu, B. Liu, M. F. C. Guedes da Silva, A. J. L. Pombeiro, *Inorg. Chim. Acta* **2009**, *362*, 2921–2926.
[48] L. Hou, D. Li, *Inorg. Chem. Commun.* **2005**, *8*, 128–130.
[49] F. R. Heirtzler, M. Neuburger, M. Zehnder, E. C. Constable, *Liebigs Ann. Recueil* **1997**, 297–301.
[50] *COLLECT Software*, Nonius BV 1997–2001.
[51] A. Altomare, G. Cascarano, G. Giacovazzo, A. Guagliardi, M. C. Burla, G. Polidori, M. Camalli, *J. Appl. Crystallogr.* **1994**, *27*, 435–435.
[52] Z. Otwinowski, W. Minor, *Methods in Enzymology*, vol. 276 (Eds.: C. W. Carter Jr., R. M. Sweet), **1997**, Academic Press, New York, pp. 307.
[53] P. W. Betteridge, J. R. Carruthers, R. I. Cooper, K. Prout, D. J. Watkin, *J. Appl. Crystallogr.* **2003**, *36*, 1487–1487.
[54] Stoe & Cie, *IPDS* software v. 1.26, Stoe & Cie, Darmstadt, Germany, **1996**.
[55] G. M. Sheldrick, *Acta Crystallogr., Sect. A* **2008**, *64*, 112–122.
[56] I. J. Bruno, J. C. Cole, P. R. Edgington, M. K. Kessler, C. F. Macrae, P. McCabe, J. Pearson, R. Taylor, *Acta Crystallogr., Sect. B* **2002**, *58*, 389–397.
[57] L. J. Farrugia, *J. Appl. Crystallogr.* **1997**, *30*, 565–565.

Received: February 21, 2010
Published Online: March 23, 2010

